ELSEVIER

Journal of Hydrology 215 (1999) 188–201

Journal of Hydrology

# Modeling solute transport in a water repellent soil

H.V. Nguyen[a,*], J.L. Nieber[a], P. Oduro[a], C.J. Ritsema[b], L.W. Dekker[b], T.S. Steenhuis[c]

[a]*Department of Biosystems and Agricultural Engineering, University of Minnesota, St. Paul, MN, USA*
[b]*DLO Winand Staring Centre for Integrated Land, Soil and Water Research, Wageningen, The Netherlands*
[c]*Department of Agricultural and Biological Engineering, Cornell University, Ithaca, NY, USA.*

Received 9 May 1998; accepted 24 August 1998

**Abstract**

A bromide tracer was applied on a 2.2 m long and 0.4 m wide plot at the location of a hydrophobic soil in the southwest of The Netherlands. At the end of the experiment, the plot was excavated to a depth of 0.7 m using 100 $cm^3$ samples, yielding a total of 1680 samples to quantify the three-dimensional spatial distribution of water content, pH, bromide concentration and degree of water repellency. Measured water content and solute distributions indicated that unstable (fingered) flow prevails. It is considered that contaminant transport under such conditions can proceed at rates that are higher than that which would normally occur if the flow were stable. This article illustrates an attempt at modeling contaminant transport under unstable flow conditions using measurements obtained from the experimental plot. A finite element solution of the two-dimensional Richards equation forms the basis for the unstable flow simulation, while a particle tracking random walk solution of the two-dimensional convection–dispersion equation forms the basis of the transport simulation. The water flow simulation and the solute transport simulation were compared with the measured data. Initial results indicate that model predictions compared fairly well with measured water content and solute transport data. 

*Keywords:* Unstable flow; Preferential flow; Hydrophobic soil; Solute transport; Particle tracking method

## 1. Introduction

The contamination of groundwater by substances from various point and non-point sources is a significant problem. Many aquifers have been invaded by anthropogenic chemicals resulting from leaky underground storage tanks, chemical spills, waste landfills and agricultural production. These pose dangers to the drinking water resources in many parts of the world. Numerical simulation models offer an effective tool for predicting the movement of contaminants and evaluating the sensitivity of the governing contaminant transport processes to their inherent system parameters.

In recent times however, models based on diffuse types of flows and solute transport have often been found to be incapable of simulating actual water flow and solute transport. The occurrence of preferential flow is the main reason for this shortcoming (Ritsema and Dekker, 1998). Preferential flow generally occurs when there are macropores, but in the absence of macropores it has been observed to occur when conditions that promote instability at the wetting front are present (Hill and Parlange, 1972; Diment et al., 1982; Glass et al., 1988; Ritsema and Dekker, 1994). In the latter case, the resulting flow is termed unstable.

When unstable flow occurs, water and solutes move

* Corresponding author. Tel.: + 1-612-625-6724; Fax: + 1-612-624-3005; e-mail: hnguyen@s1./arc.umn.edu

0022-1694/99/$ - see front matter 
PII: S0022-1694(98)00270-4

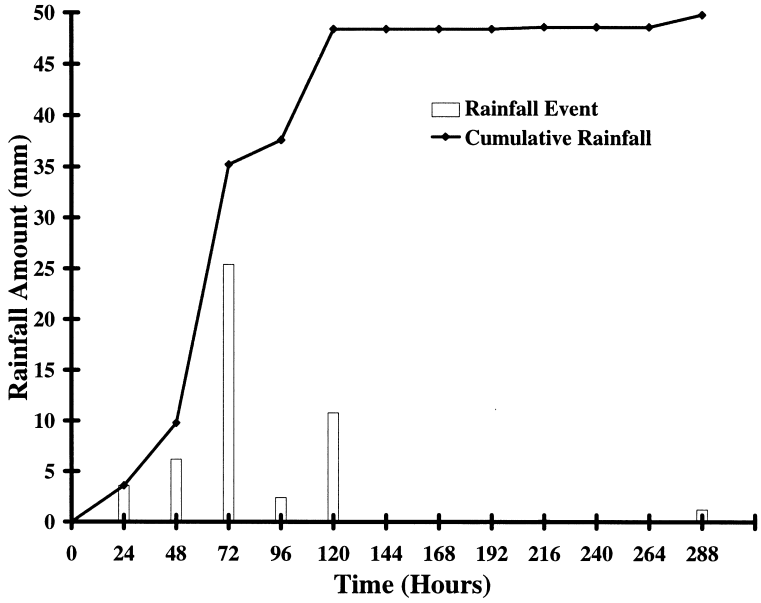


Fig. 1. Rainfall event and cumulative amounts from November 15 to 27, 1995.

in preferential pathways through the vadose zone at velocities that are close to the saturated pore velocity (Glass et al., 1988). This by-passing flow can significantly increase the amount of harmful substances moving to the underlying groundwater (Glass et al., 1988), and also cause a reduction of nutrients and water available for plant growth (Jamison, 1945). Thus, it is necessary to develop tools for modeling solute transport under unstable flow conditions for possible incorporation into existing models.

In the development of models for simulating unstable flow, Nieber (1996) proposed a numerical solution scheme of the Richards equation to model unstable flow. He showed that the model was capable of predicting finger widths that were similar to those obtained from analytical theory. Nguyen et al. (1999) successfully demonstrated modeling of unstable flow using the methodology of Nieber (1996) for field conditions.

The purpose of this article is to report on attempts to simulate solute transport patterns observed in the field under unstable flow conditions in a water repellent soil. The simulation of the observed wetted patterns is achieved with a finite element solution of the two-dimensional Richards equation. Solute transport is modeled using the random walk particle tracking (RWPT) model to solve the convection–dispersion equation. The particle tracking method has the advantage (over finite difference approximations and finite element methods) of being able to overcome numerical dispersion and artificial oscillations associated with sudden spatio–temporal changes in solute concentration (Abulaban et al., 1998). Clearly, modeling solute transport under unstable flow conditions will involve sudden changes in solute concentration at the wetting front. In this article, model results are compared with field measured data from a bromide tracer experiment on a water-repellent soil in The Netherlands.

## 2. Materials and methods

### *2.1. Field experiments*

#### *2.1.1. Soil*

The experimental site is located near Ouddorp in the southwestern part of The Netherlands. The soil consists of approximately 10 cm organic rich topsoil upon fine medium dune sand, and has been classified as a Typic Psammaquent (De Bakker, 1979). Beneath the humic layer, the soil is water repellent to a depth

of more than 50 cm. The experimental site is grass covered, and was previously used in a detailed TDR experiment on finger formation and finger recurrence using an automated TDR measuring device (Ritsema et al., 1997a), and a subsequent modeling study (Nguyen et al., 1999).

#### 2.1.2. Tracer experiment

The experimental plot was 2.2 m long and 0.4 m wide. A KBr tracer solution was applied manually to the soil surface with six nozzle sprinklers on November 15, 1995. The tracer application rate was determined by placing 24 small trays around the experimental plot. An average of 8.0 g bromide per $m^2$ was applied, with a standard deviation of 1.5 $g/m^2$. On November 27, after 52 mm of rain, excavation of the experimental plot was performed, according to a spatial grid of 40 × 6 × 7 samples, in the *x*, *y* and *z* directions, respectively, yielding a total of 1680 samples for the entire plot. Samples were taken by using steel cylinders (5 cm high by 5 cm diameter; or about 100 $cm^3$ volume), which were carefully pushed into the soil. In the horizontal direction, the separation distance between two adjacent samples was 0.5 cm. Seven soil layers were sampled at depth intervals of 0–5, 9–14, 19–24, 30–35, 42–47, 55–60, and 69–74 cm. The samples were taken to the laboratory for the determination of soil water content, degree of water repellency, soil pH, and bromide concentration. In this article, soil water content and bromide concentration distributions will be used.

Rainfall and groundwater levels were recorded automatically from November 15 to 27. A total of 52 mm of rain was recorded in this period, and the groundwater table rose from a depth of about 174 to 170 cm below the soil surface. A plot of the rainfall event and cumulative rainfall amount are shown in Fig. 1.

### 2.2. Laboratory measurements

All field-moist soil samples were first weighed in the laboratory, and the degree of actual water repellency was determined using the water drop penetration time (WDPT)-test described by Dekker and Ritsema (1994). Thereafter, samples were oven-dried at 65°C, and weighed again to determine the volumetric soil water content. The samples were then used to determine bromide concentrations. After adding water to the samples, and shaking for a fixed period of time, bromide concentration in the solution was measured using the High Pressure Liquid Chromatography technique.

### 2.3. Numerical methods

#### 2.3.1. Numerical method for unstable flow

The numerical simulation of the flow of water in the experimental trench is based on a finite element solution of the two-dimensional Richards equation. The derivation of the finite element equations was presented by Nieber (1996). Details of the application of this numerical solution to the experimental trench were presented by Nguyen et al. (1999).

The numerical solution to the Richards equation provides data on the distribution of water pressure and water saturation in the soil profile. To perform the solute transport simulation, it is necessary to compute the pore velocities within the flow domain. These velocities are derived from the finite element solution results by applying Darcy's law as:

$$\theta v_x = -K\frac{\partial h_w}{\partial x}, \tag{1a}$$

$$\theta v_z = -K\frac{\partial h_w}{\partial z} - K, \tag{1b}$$

where $\theta$ is the volumetric water content, $v_x$ and $v_z$ are the horizontal and vertical velocities, $K$ is the unsaturated hydraulic conductivity, $h_w$ is the water pressure, and $x$ and $z$ are the horizontal and vertical Cartesian coordinates, respectively.

#### 2.3.2. Numerical method for solute transport

The transport of a non-sorbing solute can be solved numerically using the convection–dispersion equation (CDE) under unsaturated conditions. It is written as:

$$\frac{\partial \theta C}{\partial t} + \nabla\cdot(\theta C v) - \nabla\cdot(\mathbf{D}\cdot\theta\nabla C) = 0, \tag{2}$$

where $C$ is the solute concentration in the liquid phase, $\mathbf{D}$ the hydrodynamic dispersion tensor defined by Eq. (3), $\mathbf{v}$ is the local velocity vector, and $t$ is the time. The hydrodynamic dispersion tensor is given by

$$\mathbf{D} = (\alpha_T V + D_m)\mathbf{I} + (\alpha_L - \alpha_T)\frac{\mathbf{vv}}{V}, \tag{3}$$

where $\alpha_L$ and $\alpha_T$ are the longitudinal and transverse dispersivities respectively, $V$ is the magnitude of the velocity vector, $D_m$ is the molecular diffusion coefficient, $\mathbf{I}$ is the identity matrix, and $\mathbf{vv}$ is the diadic of the velocity vector.

The RWPT method can be used to obtain a solution to Eq. (2). In this method, a mass of solute is represented by a finite number of discrete particles that move with a convective force represented by the local velocity field, and a dispersive component that is represented as a random movement. To solve the CDE by the RWPT method, Eq. (2) may be rearranged in a form similar to the Fokker–Planck equation, that is,

$$\frac{\partial(\theta C)}{\partial t} + \nabla\cdot\left[\theta C\left(v + \frac{1}{\theta}\mathbf{D}\cdot\nabla\theta\right)\right] - \nabla\cdot\{\mathbf{D}\cdot\nabla(\theta C)\} = 0. \tag{4}$$

The Fokker-Planck equation is given by Eq. (5) (Tompson et al., 1988), and is a conservation equation for the probability distribution of particles moving independently in a random field.

$$\frac{\partial f}{\partial t} + \nabla\cdot\left[f\mathbf{A} - \nabla\cdot\left(\frac{1}{2}\mathbf{B}\mathbf{B}^{\mathrm{T}}\right)\right] - \nabla\cdot\left\{\frac{1}{2}\mathbf{B}\mathbf{B}^{\mathrm{T}}\cdot\nabla f\right\} = 0. \tag{5}$$

In Eq. (5), $f(\mathbf{X},t)$ is the probability density of particles expected to be found around a location $\mathbf{X}$ at time $t$, $\mathbf{X}(t)$ is the position of a particle at time $t$, $\mathbf{A}(\mathbf{X},t)$ is the vector used to represent the deterministic driving force acting to change $\mathbf{X}$, and $\mathbf{B}(\mathbf{X},t)$ is a second order tensor aligning the random forces acting on the particle with $\mathbf{A}$. The location of a particle, $i$, that moves in a random field at time $t$, can be described by the integrated form of the non-linear Langevin equation (Gardiner, 1985) over a time step $\Delta t_m$ as

$$\mathbf{X}_{m,i} = \mathbf{X}_{m-1,i} + \mathbf{A}_i\Delta t_m + \mathbf{B}_i\mathbf{R}_{m,i}\sqrt{\Delta t_m}, \tag{6}$$

where the subscript $m$ indicates the time level, $\mathbf{X}_{m,i}$ and $\mathbf{X}_{m-1,i}$ are subsequent locations of particle $i$ over a time interval $\Delta t_m\,(=\,t_m\,-\,t_{m-1})$. In this article, the vector $\mathbf{R}_{m,i}$ is represented by a simple uniform distribution $U(\pm\sqrt{3})$ for each component, $\mathbf{R}_{m,j,i}\,(j\,=\,x,z)$ of $\mathbf{R}_{m,i}$.

Comparison of Eq. (2) with Eq. (5) indicates that the terms $\mathbf{A}$ and $\mathbf{B}$ must be chosen such that

$$f = \theta C, \tag{7a}$$

$$\mathbf{B}\mathbf{B}^{\mathrm{T}} = 2D \tag{7b}$$

$$\mathbf{A} = \mathbf{v} + \nabla\cdot\mathbf{D} + \frac{1}{\theta}\mathbf{D}\cdot\nabla\theta. \tag{7c}$$

If a large number of particles represent a fixed amount of total solute mass, then the location of any particle can be found in the form of a stepping equation as

$$\mathbf{X}_{m,i} = \mathbf{X}_{m-1,i} + \left[\mathbf{v}(\mathbf{X}_{m-1,i},t_m) + \nabla\cdot\mathbf{D}(\mathbf{X}_{m-1,i},t_m) + \frac{1}{\theta}\mathbf{D}(\mathbf{X}_{m-1,i},t_m)\cdot\nabla\theta\right]\Delta t_m + \mathbf{B}(\mathbf{X}_{m-1,i},t_m)\mathbf{R}_{m,i}\sqrt{\Delta t_m} \tag{8}$$

A more detailed explanation of the solution technique of RWPT method can be found in Tompson et al. (1988) and Abulaban et al. (1998). Abulaban et al. (1998) developed a RWPT code for solute transport in saturated porous media. For use in the present study, this code was modified to accommodate the simulation of solute transport in unsaturated porous media, that is the solution of Eq. (2). Conditions for both instantaneous sources and continuous sources of solute were accommodated in the code. Ahlstrom et al. (1977) discusses in detail the application of the method to the case of a continuous source. The particles were uniformly initiated in the top boundary and could leave the domain only at the bottom boundary during the simulation period.

### 2.4. Model evaluation

To determine how well the numerical simulations of flow and solute concentrations mimic the observed field data, visual comparisons of observed and simulated patterns of wetting and solute concentration were performed. In addition, three statistical measures of the comparison of the observed and simulated water content and solute concentration were calculated. These were the mean difference (MD) between the simulated and observed values, standard deviation for the mean difference (S) and coefficient of determination (CD). The equations for these measures are presented by Nguyen et al. (1999) and the background justification for their use is given by Cooley (1979) and Loague and Green (1991).

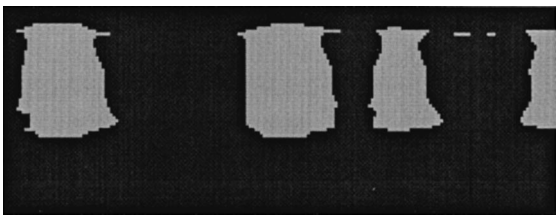

Fig. 2. Illustration of zonal designation of initial conditions assigned for the water flow simulation.

## 3. Modeling of unstable flow and solute transport

As the flow and solute transport models were two-dimensional models, model results will be compared with field data from two-dimensional sections (vertical slices) of the three-dimensional domain. The bromide tracer experiment was performed over a 12-d period. At the end of this period, the soil profile was excavated to measure the distribution of water content and solute concentration. While model simulations of saturation and solute concentration are available over the 12-d period of the tracer experiment, only the

Table 1
Distribution of number of particles injected during the simulation period.

| | Number of particles | |
|---|---|---|
| Date | Scenario 1 | Scenario 2 |
| 11/15/95 | 50 000 | 3557 |
| 11/16/95 | | 6126 |
| 11/17/95 | | 25 098 |
| 11/18/95 | | 2371 |
| 11/19/95 | | 10 672 |
| 11/23/95 | | 198 |
| 11/26/95 | | 1186 |
| 11/27/95 | | 792 |

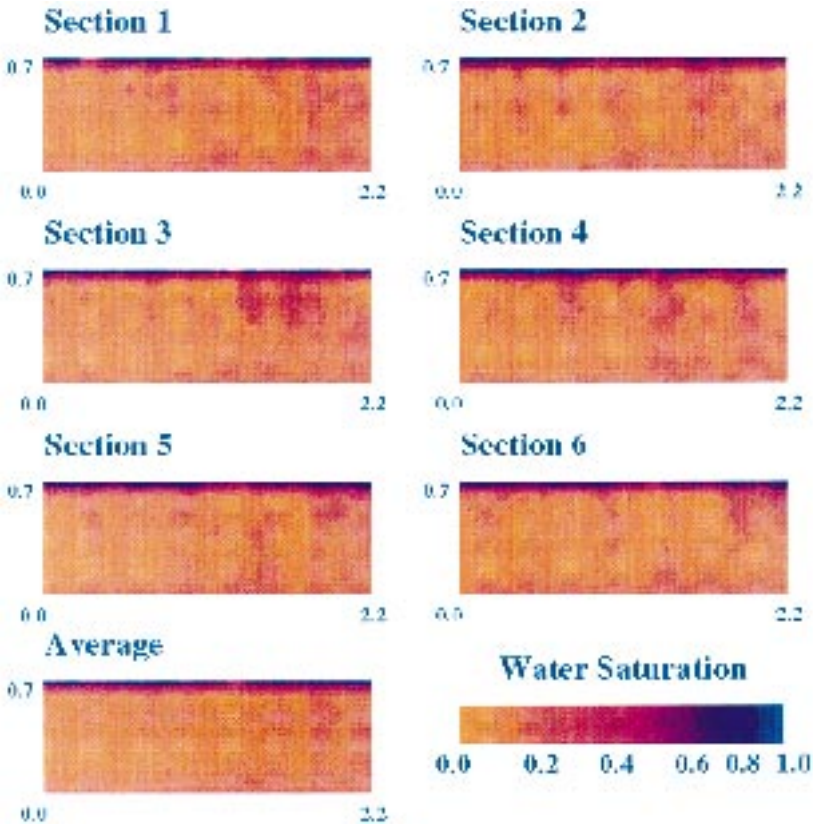


Fig. 3. The spatial distribution of observed saturation for the six sections.

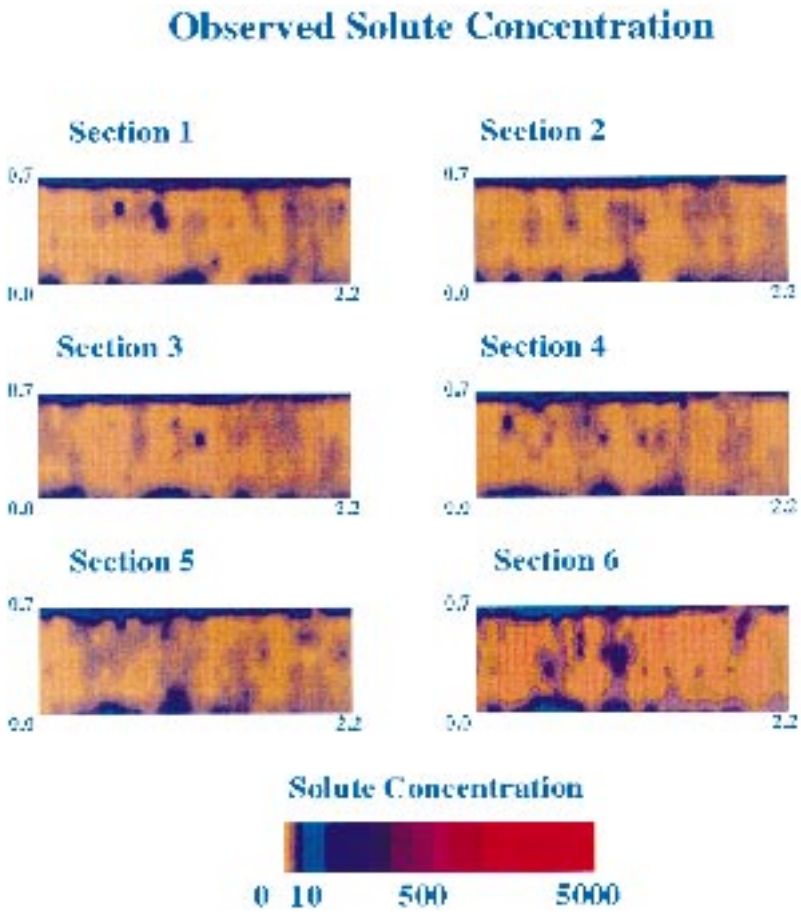


Fig. 4. The spatial distribution of observed solute concentration for the six sections.

simulated results on the 12th day will be used for comparison with the field data.

The two-dimensional flow domain ($2.2 \times 0.7\ m^2$) was discretized into 14 000 linear rectangular elements with vertical and horizontal dimensions of 0.01 and 0.011 m, respectively. The soil parameters used in the simulations and the implementation of the initial and boundary conditions are summarized in Nguyen et al. (1999). The velocities and volumetric water content obtained from the unstable flow model for all elements were used as input for the solute transport model.

The initial condition for the water flow simulation requires assignment of water saturation and position on the hysteric water retention curve for the soil. The initial saturation distribution was identical to that used by Nguyen et al. (1999). Assignment of the initial position on the water retention curve was based on the pattern of wetting observed (and simulated) to occur in the trench as reported by Nguyen et al. (1999). It was assumed that the soil in the zones previously wetted (by finger flow) would experience the drainage cycle of the water retention curve, while the soil in the zones that had remained dry (zones between the fingers) would experience the wetting cycle of the water retention curve. A schematic of the assigned zones is shown in Fig. 2. The darker color represents portions assigned to the main drainage curve and the lighter color, the main wetting curve. These assigned initial conditions essentially

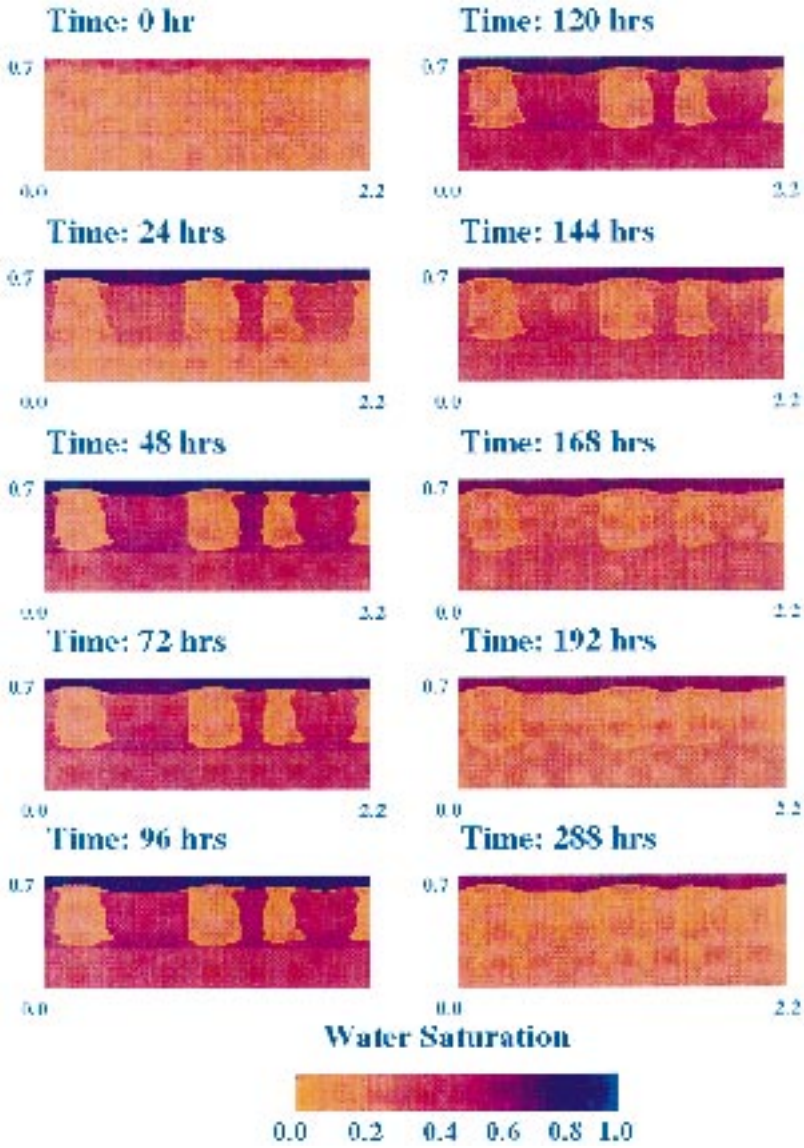


Fig. 5. The distributions of simulated saturation at various times and the distribution of average observed saturation for the six sections.

predetermine that the water will flow preferentially down the previously wetted zone because of finger persistence (Glass et al., 1989; Nieber, 1996). As the objective of this study was to test the preferential transport of the solute, this predetermined condition was not considered a limitation of the study.

The solute transport simulations were performed several times to test the effect of the longitudinal dispersivity, $\alpha_L$ assigned to the discrete element domains. Values used ranged between 0.001 and 0.01 m, a range in accord with the recommendations of Fried (1975) and common practice. We found that using the value of 0.001 m, led to insufficient spread of the solute in comparison to the observed solute distribution. A longitudinal dispersivity of 0.01 m yielded solute plumes in much better agreement

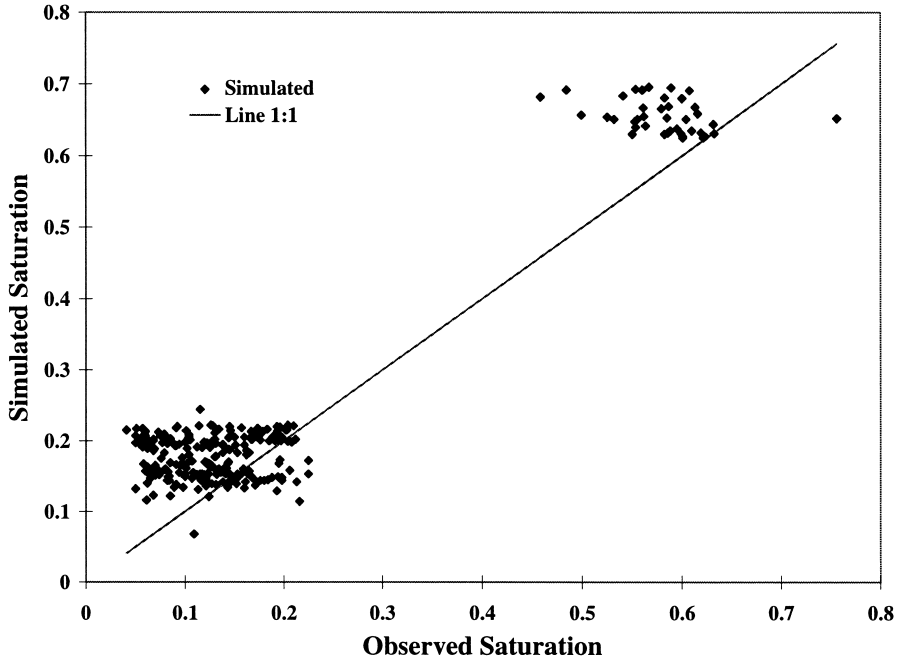


Fig. 6. Observed versus simulated saturation at sampling locations.

with the measured solute plume and therefore, the results reported here will be for $\alpha_L = 0.01$ m. The transverse dispersivity, $\alpha_T$, was set equal to 0.2 $\alpha_L$ ( = 0.002 m), also in accord with the common practice.

The solute mass was represented by 50 000 particles. Two scenarios were run: (1) particles were instantaneously injected at the beginning of the simulation and (2) particles were successively injected in proportion to the rainfall amount. In the first scenario, the assumption was that all solute were fully mixed with the initial soil water and transport of the whole mass proceeded immediately upon injection. In scenario (2), the assumption was based on a suggestion to account for the observed high concentration of bromide in the humic layer. Ritsema and Dekker (1998) proposed that the humic layer acted like a reservoir of bromide, releasing it through lateral spreading to the finger pathways for vertical migration to the bottom of the profile. Successive injection was then a means of simulating this ''reservoir of bromide''. In both scenarios, the particles were initiated from the elements at the surface. Table 1 shows the distribution of particle injection over the simulation period.

## 4. Results and discussion

### 4.1. Observed saturation and solute concentration

The observed saturation and bromide concentration patterns were displayed for six vertical planes ($x$–$z$ domains) in which the $y$-horizontal locations were 2.7, 8.5, 14.2, 20.0, 25.7 and 31.5 cm. These six sections were numbered 1, 2, 3, 4, 5 and 6, respectively. The soil water content for the 280 soil samples for each section was converted to saturation data. These saturation and solute concentration data were interpolated by Kriging method using SURFER™ software (version 5.0).

Illustrations of the observed spatial pattern of moisture saturation in the six sections are presented in Fig. 3, while the observed solute concentration in these sections are presented in Fig. 4. It is seen from these plots that the patterns of saturation and solute concentration are quite similar in spatial distribution. Most values of solute concentration and saturation were smaller than 10 g/m$^3$and 0.3, respectively, in the hydrophobic layer. The saturation and solute concentration were high in the humic layer and in

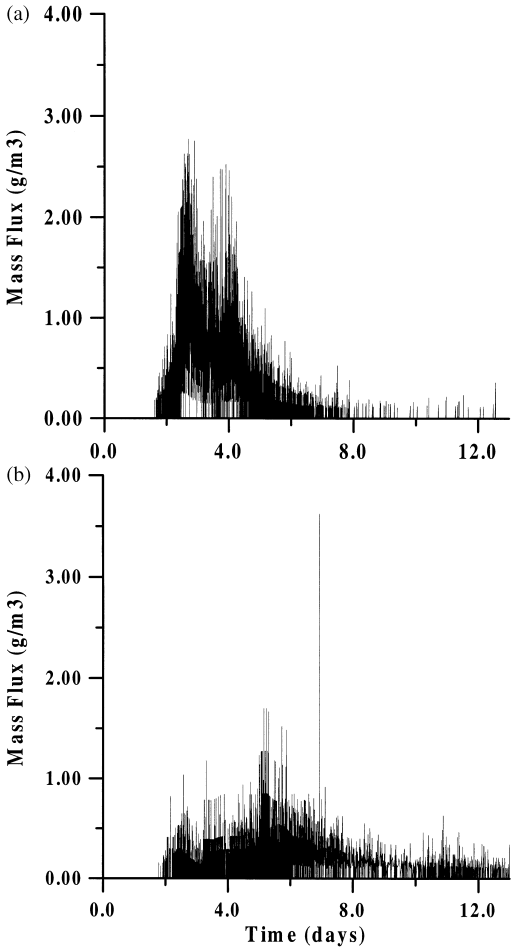


Fig. 7. (a) The breakthrough curve at the bottom of soil profile for scenario (1); (b) the breakthrough curve at the bottom of soil profile for scenario (2).

the 60–70 cm depth layer relative to the rest of the domain. The total mass of bromide left in the soil profile was computed from the six sections to be 4.752 g. The total solute mass applied at the surface was 7.04 g, and therefore it was estimated that the amount of bromide leached through the bottom of the profile was 2.288 g, or 32.5% of the applied mass.

### *4.2. Simulation of water saturation*

Fig. 5 shows the simulated saturation at various times. After 24 h, and 4 mm of rainfall, the infiltrating rainfall had moved into the fingered paths and the wetting front had already reached the underlying hydrophilic layer. The water in these fingered pathways did not diffuse laterally because of the poor wettability of the surrounding hydrophobic media. After 48 h, and 10 mm of cumulative rainfall, the infiltrating water had penetrated into the underlying hydrophilic layer and it could be seen that the wetting pattern had spread widely in the hydrophilic layer. These observations were similar to those found in the field by Ritsema et al., 1993 (see their Fig. 13).

From 48 to 120 h, an additional 40 mm of rainfall accumulated, and this water continued to move downward from the surface through the fingered pathways to the hydrophilic layer. Following this rainfall, the profile drained. In the drained profile, shown at 192 h, it is difficult to distinguish the fingered flow paths observed earlier. This indicated that most of the water had drained within the 120 h following the last major rain event. This generally agrees with the observations from the field showed by Ritsema et al., (1997a,b)). Only trace amounts of rain occurred after the last major rain event and the redevelopment of the preferential flow paths barely became visible. The amount of additional rainfall was too small to promote complete renewal of these pathways.

The observed wetted patterns shown in Fig. 3 correspond to the simulated saturation pattern shown in Fig. 5 at 288 h. In general, both the observed and simulated saturation patterns show that the saturation was high in the humic layer and near the bottom of the soil profile. The biggest discrepancies between the observed and simulated saturation distributions occur in the hydrophobic layer. The simulated wetted regions appear to be somewhat wider than those in the observed regions. This may be caused by the fact that in the assignment of the properties of the hydrophobic layer, it was

Table 2
Summary of statistical analyses of differences between simulated and observed saturation and solute concentration.

| Statistic | Saturation[a] | Solute concentration[b] |
|---|---|---|
| MD | 0.054 | − 5.058 |
| S | 0.055 | 7.470 |
| CD | 0.864 | 1.078 |

[a] $n = 280$
[b] $n = 272$.

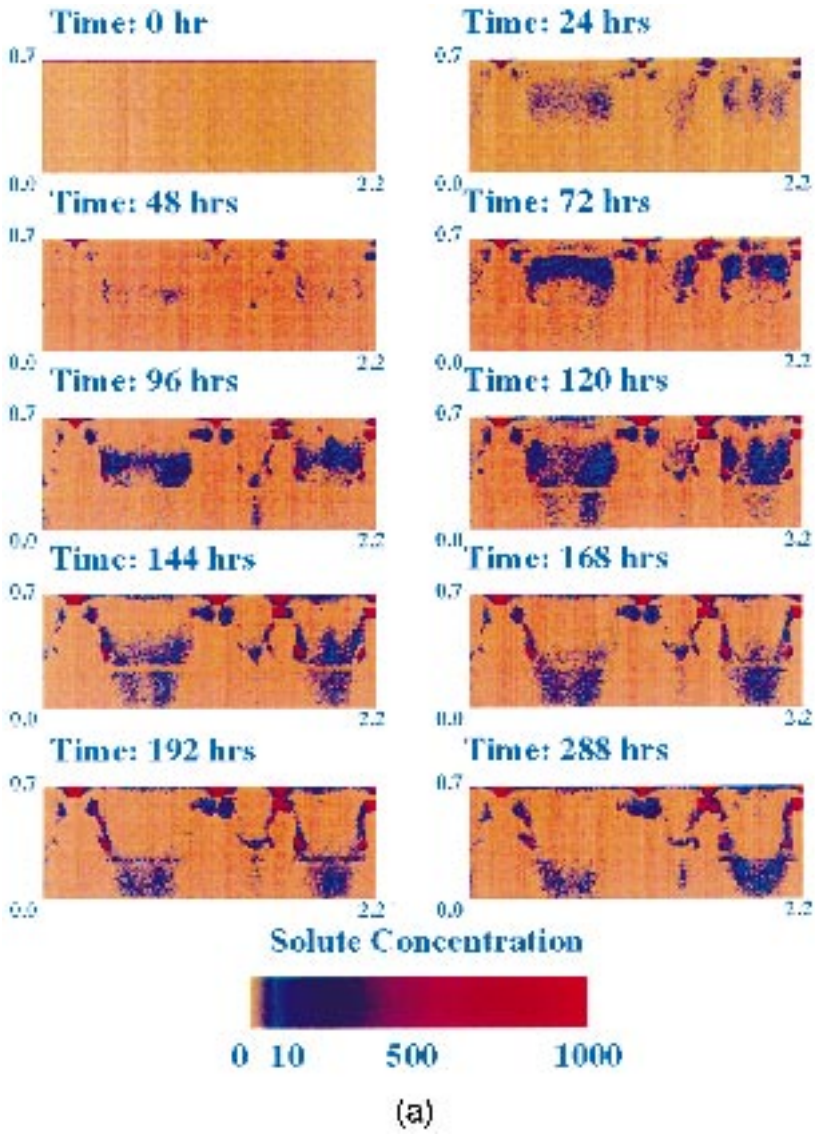


Fig. 8. (a) The spatial distribution of simulated solute concentration for scenario (1); (b) the spatial distribution of simulated solute concentration for scenario (2).

assumed that the properties were spatially uniform. We hypothesize that the somewhat narrower wetted zones in the observed saturation distribution may be due to the fact that the hydrophobic layer has a non-uniform distribution of wettability as shown by Ritsema and Dekker (1998).

The observed saturation was sampled at a scale of 5 cm in the vertical and horizontal directions, and so to compare with the measured values the simulated results were averaged over the same scale. A plot of the observed versus simulated saturation at the sampling locations is presented in Fig. 6. The average observed saturations for the six sections were used for this plot. As the water content in the soil profile is either dry (inter-finger zones) or wet (finger zones or humic layer), the predicted saturation distributed separately in two zones: low and high saturation (Fig. 6). The difference between simulated and

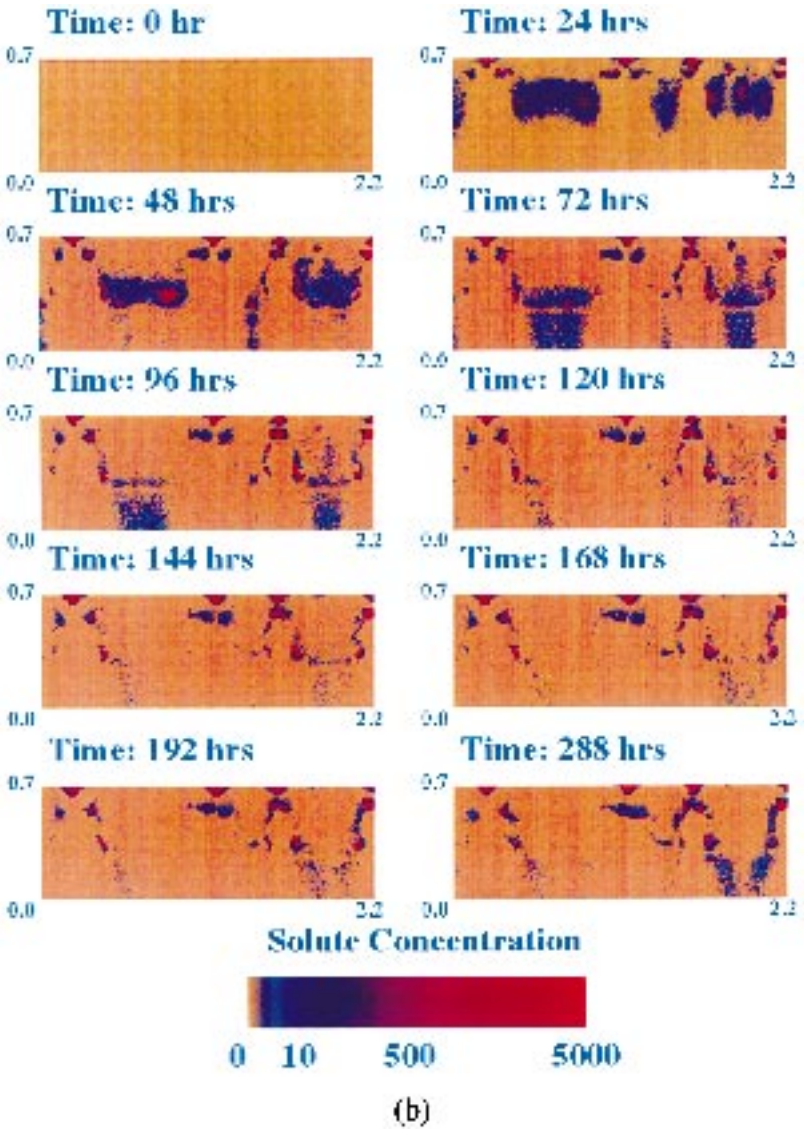


Fig. 8. (*continued*)

observed saturation ranged between −10% and +15%.

The result of the statistical analyses is summarized in Table 2. The unstable flow model over-predicted the saturation by approximately 5% (MD = 0.054) with standard deviation (S = 0.055) of 5.5%. The proportion of the total variance of observed data explained by the predicted data was 0.864 (CD). In general, we can conclude that the unstable flow model predicted soil saturation values that were in reasonably good agreement with what was observed.

### *4.3. Simulated bromide concentration*

Figs. 7(a) and (b) show the breakthrough curves at the bottom of the soil profile for the two scenarios. The mass of bromide that had left the domain can be computed by integrating the plot of mass flux over

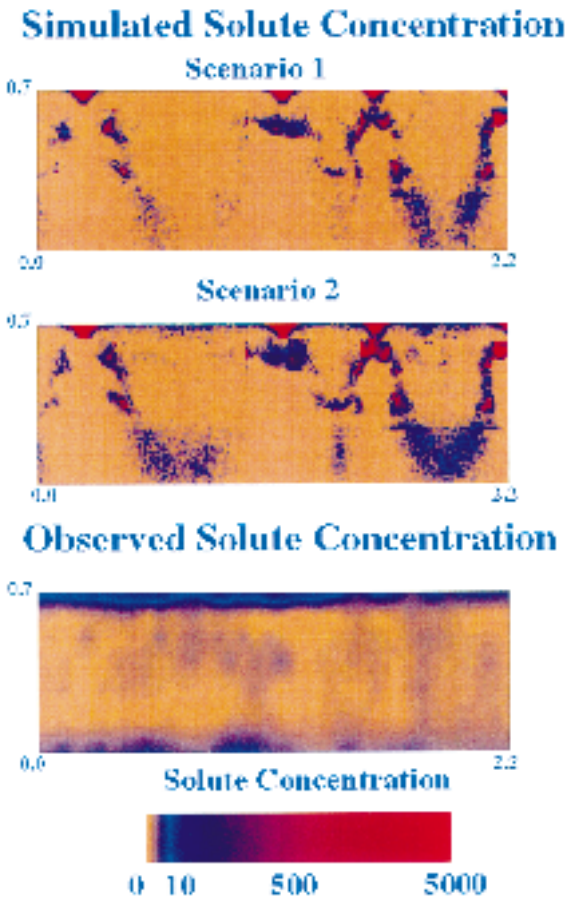


Fig. 9. The distribution of simulated solute concentration at 288 h and average measured solute concentration for the six sections.

time. The amount of bromide leached out of the profile for both scenarios compared very well with the observed. For scenario (1), 31.2% of the total injected mass left the profile and for scenario (2), 27.1% left. These quantities compare quite well with the observed amount of 32.5%. The breakthrough curves for the two scenarios differ in the time distribution of mass flux leaving the profile. Scenario (1) shows a very prominent peak which tails off appreciably towards the end of the simulation period, while scenario (2) shows a flatter peak which is delayed relative to scenario (1), has very little variation in the mass flux, and does not tail off as much toward the end of the simulation period.

The pattern of simulated solute migration is seen to be similar to that of the simulated water migration, as expected. Figs. 8(a) and (b) show the patterns of simulated solute concentration at various times for the two scenarios. The solute particles reached the hydrophobic layer at 24 h, and some left the bottom of the soil profile at 48 h in both the scenarios. The mass flux for scenario (1) is higher than that for scenario (2) until 120 h. It is reversed after that time. As the saturation and velocity distributions are the same for both scenarios, the differences between these is owing to the mode of solute injection for the two scenarios. Visual assessment of the concentration profiles of the two scenarios shows that there was little difference between them. At the end of the simulation, scenario (1) showed solute remaining in a few spots in the humic layer, while scenario (2) has solute distributed fairly uniformly within the humic layer. There is more solute left in the hydrophilic layer for scenario (2) than for scenario (1).

The simulated solute distributions for the two scenarios at 288 h are presented in Fig. 9, with the distribution of average solute concentration for the six sections. There is considerable difference in the point by point solute concentration between the simulated and observed solute distributions. In particular, we can see that there is significantly more solute remaining in the humic layer than is found in the simulated results, and there seems to be more observed lateral spreading of the solute in the hydrophilic layer than found in the simulated results.

The results of the statistical analyses comparing the solute distributions for scenario (2) at 288 h with the average measured results are summarized in Table 2. Scenario (2) was selected because the observed solute distribution pattern in the humic layer was better represented in this scenario than in scenario (1). In the calculation of the statistics for the comparison of the simulated and observed solute concentrations, eight of he 280 sampling values were not used because they were extreme outliers (the simulated values were approximately one order of magnitude larger than the observed). The model underpredicted solute concentration (MD = − 5.06). The large value of S (7.470) indicates that the variation between observed and simulated solute concentration is high. The proportion of the total variance of observed data explained by the predicted data was close to one (CD = 1.078), signifying model performance to be fairly good. Fig. 10 helps to explain these statistical

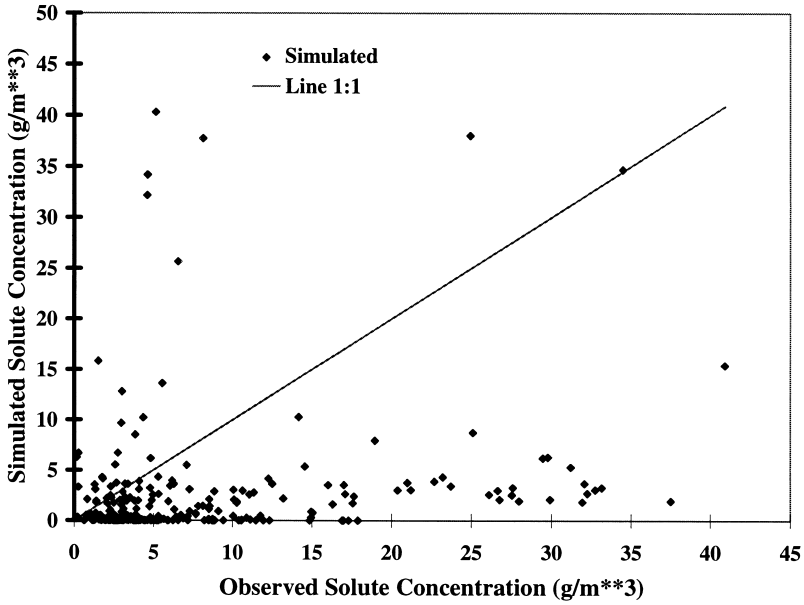


Fig. 10. Observed versus simulated solute concentrations at the sampling locations.

measures. This figure shows the observed versus simulated solute concentration at sampling locations. In general, the difference between the simulated and observed solute concentration was quite small.

## 5. Conclusions and future work

(1) The unstable flow model predicted water saturations reasonably close to those measured at the measurement points at the time of the plot excavation. This result is in agreement with the results shown by Nguyen et al. (1999).

(2) The modeling effort showed that solute concentration patterns under unstable flow conditions could be captured with some degree of success, but to a lesser extent than that shown for the water saturation distribution. It was found that the best transport simulation resulted when the solute was injected proportionally to the amount of rainfall rather than being instantaneously injected at the beginning of the simulation. This may indicate partial mixing of the applied solute and indicate that subsequent rainfall events are required to mobilize all the applied solute.

(3) In both scenarios, the quantity of solute that is leached out of the profile is quite close to that observed. This result is quite gratifying considering that this was a first effort to model such a complex phenomenon.

(4) In future work, we intend to examine the effect of heterogeneous wettability of the hydrophobic layer on the patterns of water flow and solute transport in the soil profile at this site.

## Acknowledgements

Published as Paper No. 981120024 of the scientific journal series of the Minnesota Agricultural Experiment Station on research conducted under Minnesota Agricultural Experiment Station. This study was executed within the framework of (i) the Environment and Climate Research Program of the European Union, as part of the research project ‘Analysis and improvement of existing models of field scale solute transport through the vadose zone of differently textured soils with special reference to preferential flow’, and (ii) the Research Program 223 ‘Physical Soil Quality’ of the Dutch Ministry of Agriculture, Nature Management and Fisheries. The modeling part was supported by the Army High Performance Computing Research Center under the auspices of

the Department of the Army, Army Research Laboratory cooperative agreement number DAAH04-95-2-0003/contract number DAAH04-95-C-0008, the content of which does not necessarily reflect the position or the policy of the government, and no official endorsement should be inferred. Collaboration on the research was supported by the NATO Collaborative Research Grant No. 960704.

## References

Abulaban, A., Nieber, J.L., Misra, D., 1998. Modeling plume behavior for nonlinearly sorbing solutes in saturated homogeneous porous media. Advances in Water Resources 21, 487–498.

Ahlstrom, S.W., Foote, H.P., Arnett, R.C., Cole, C.R., Serne, R.J., 1977. Multicomponent mass transport model: theory and numerical implementation. Report BNWL 2127, Battelle, Pacific Northwest Laboratories, Richland WA.

Cooley, R.L., 1979. A method of estimating parameters and assessing reliability for models of steady state groundwater flow, 2: application of statistical analysis. Water Resour. Res. 15 (3), 603–617.

De Bakker, H., 1979. Major soils and soil regions of the Netherlands. Junk, Den Haag and Pudoc, Wageningen, the Netherlands.

Dekker, L.W., Ritsema, C.J., 1994. How water moves in a water repellent sandy soil. 1. Potential and actual water repellency. Water Resour. Res. 30, 2507–2517.

Diment, G. A., Watson, K.K., Blennerhassett, P.J., 1982. Stability analysis of water movement in unsaturated porous materials, 1. Theoretical considerations. Water Resour. Res. 18, 1248–1254.

Fried, J.J., 1975. Groundwater Pollution. Elsevier, NY.

Glass, R.J., Steenhuis, T.S., Parlange, J.-Y., 1988. Wetting front instability as a rapid and far-reaching hydrologic processes in the vadose zone. J. Contam. Hydrol. 3, 207–226.

Glass, R.J., Steenhuis, T.S., Parlange, J.Y., 1989. Mechanism for finger persistence in homogenous, unsaturated, porous media: Theory and verification. Soil Sci. 148, 60–70.

Hill, D.E., Parlange, J.-Y., 1972. Wetting front instability in layered soils. Soil Sci. Soc. Am. Proc. 36, 697–702.

Jamison, V.C., 1945. The penetration of irrigation and rain water into sandy soils of central Florida. Soil Sci. Soc. Amer. Proc. (10), 25–29.

Loague, K.M., Green, R.E., 1991. Statistical and graphical methods for evaluating solute transport models: overview and application. J. Contam. Hydrology 7, 51–73.

Nguyen, H.V., Nieber, J.L., Ritsema C.J. Dekker, L.W. Steenhuis, T.S. 1999. Modeling gravity driven unstable flow in a water repellent soil. J. Hydrol., 215, 202–214.

Nieber, J.L., 1996. Modeling finger development and persistence in initial dry porous media. Geoderma 70, 209–229.

Ritsema, C.J., Dekker, L.W., Hendrickx, J.M.H., Hamminga, W., 1993. Preferential flow mechanism in a repellent sandy soil. Water Resour. Res. 29, 2183–2193.

Ritsema, C.J., Dekker, L.W., 1994. How water moves in a water repellent sandy soil: 2. Dynamics of fingered flow. Water Resour. Res. 30, 2519–2531.

Ritsema, C.J., Dekker, L.W., van den Elsen, E.G.M., Oostindie, K., Nieber, J.L., 1997. Recurring fingered flow pathways in a water repellent sandy field soil. J. Hydrology and Earth System Sciences 4, 777–786.

Ritsema, C.J., Dekker, L.W., Heijs, A.W.J., 1997. Three-dimensional fingered flow patterns in a water repellent sandy field soil. Soil Sci. 162, 79–90.

Ritsema, C.J., Dekker, L.W., 1998. Three-dimensional patterns of moisture, water repellency, bromide and pH in a sandy soil. J. Cont. Hydr. 31(3–4): 295–313.

Tompson, A.F.B., Vomvoris, E.A., Gelhar, L.W., 1988 Numerical simulation of solute transport in randomly heterogeneous porous media: motivation, model development and application, Rep # 36, Ralph M. Parson Laboratory, Dept. of Civil Eng. Mass Inst. Of Tech. Cambridge, MA.